PHYSICS AND CHEMISTRY OF SOLID STATE
V. 27, No. 2 (2026) pp. 456-461
Section: Physics

DOI: 10.15330/pcss.27.2.456-461

Vasyl Stefanyk Carpathian National University

ФІЗИКА І ХІМІЯ ТВЕРДОГО ТІЛА
Т. 27, № 2 (2026) С. 456-461
Фізико-математичні науки

PACS: 78.70.Dm; 61.05.cp

ISSN 1729-4428 (Print)
ISSN 2309-8589 (Online)

Y.V. Zaulychnyy, V.T. Mosiak, L.O. Biriukovych, O.V. Stepanov, Y.I. Bogomol

Specific Features of Boron Detection and Interpretation in High-Entropy Borides and B_4C-Based Composites: A Brief Review

National Technical University of Ukraine "Igor Sikorsky Kyiv Polytechnic Institute", Kyiv, Ukraine,
m.vasyl-imz24@lll.kpi.ua

The specific features of detecting and interpreting boron distribution in composite materials based on boron carbide and high-entropy borides are considered. Literature data on the use of EDS and WDS methods for studying elemental distribution in high-entropy borides and B_4C–$(TiZrHfNbTa)B_2$ composites are analyzed. It is shown that the intensity of boron B Kα radiation strongly depends on the local chemical composition of the material and may significantly decrease in regions enriched with metallic components. It has been established that one of the reasons for this effect is the absorption and scattering of X-ray radiation by heavy elements, primarily zirconium, whose $M_{4,5}$ absorption edge energy is close to the energy of the boron B Kα band. As a result, regions with reduced signal intensity may appear on boron distribution maps; however, these regions do not indicate the absence of boron in the studied crystallites. The obtained results demonstrate the need to take into account the specific interaction of characteristic radiation with the components of multicomponent boride systems when interpreting X-ray spectral analysis data.

Keywords: high-entropy borides, boron carbide, EDS mapping, WDS mapping, boron distribution, B Kα radiation, X-ray spectral analysis, B_4C–$(TiZrHfNbTa)B_2$ composites, X-ray absorption.

Received 16 December 2025; Accepted 25 June 2026; Published 30 June 2026.

Introduction

Since the first studies on high-entropy alloys (HEAs) [1,2], high-entropy oxide ceramics (HEOCs) [3], and high-entropy borides (HEBs) [4], these materials have continued to attract intensive research interest. This is due to their potential use in thermal protection systems, cutting tools, and wear-resistant applications, owing to their high mechanical properties, thermal insulation capability, and thermal and corrosion resistance.

Among numerous studies on HEBs [4–23], HEB+SiC composite materials have been synthesized to strengthen these ceramics, improve their corrosion resistance, and densify their microstructure [13–19]. To modify tribological characteristics, HEB+ZrO_2 composites and HEB+h-BN compositions [23] have also been used as self-lubricating materials at high temperatures.

At the same time, the combination of the high hardness and low density of B_4C with HEBs in a composite is attractive [24] for controlling and conveniently designing thermophysical and mechanical properties that should be more compatible than those of individual HEBs. This may be useful for lightweight armor systems and other applications.

I. Analysis of the Specific Features of Detecting and Interpreting Boron Distribution in Composites

However, due to the large number of components in B_4C+HEB composites, a problem arises in identifying boron in HEB crystallites, since the emission of the B Kα band is strongly attenuated by metal atoms. Therefore, the determination of boron atom distribution simultaneously in the crystallites and in the B_4C matrix is often avoided (Figs. 1 and 2) [24,25].

It can be seen from Ref. [26] that, during the synthesis

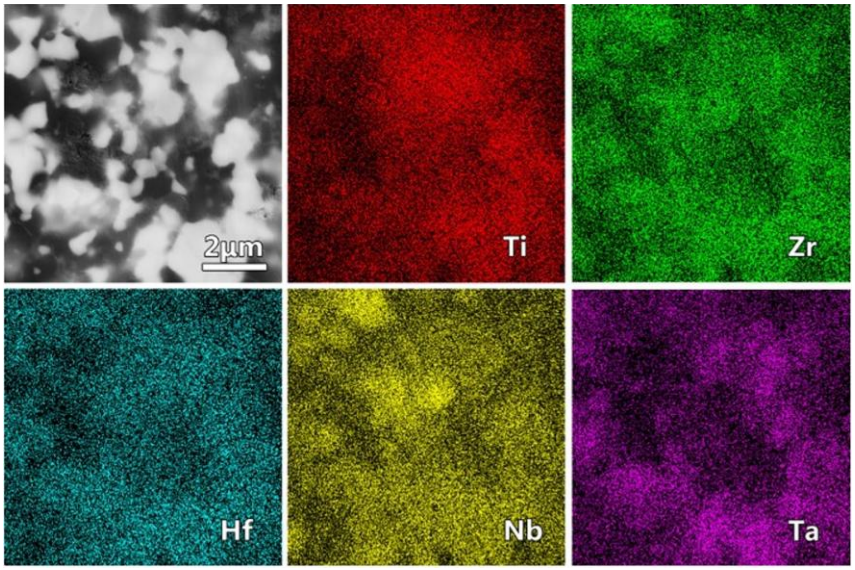

Fig. 1. SEM image and corresponding EDS mapping of Ti, Zr, Hf, Nb, and Ta elements, demonstrating Nb segregation in the HEB phase of the B_4C–$(TiZrHfNbTa)B_2$ composite [25].

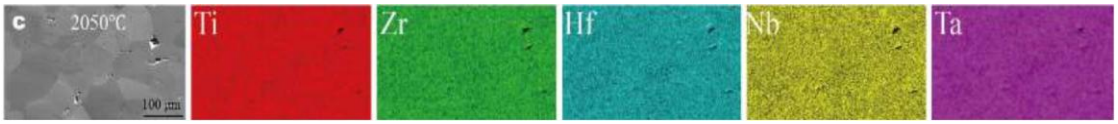

Fig. 2. WDS mapping of samples sintered at 1900 °C, 2000 °C, and 2050 °C, indicating an inhomogeneous elemental distribution at 1900 °C, whereas at 2000 °C and 2050 °C the elemental distribution is homogeneous [25].

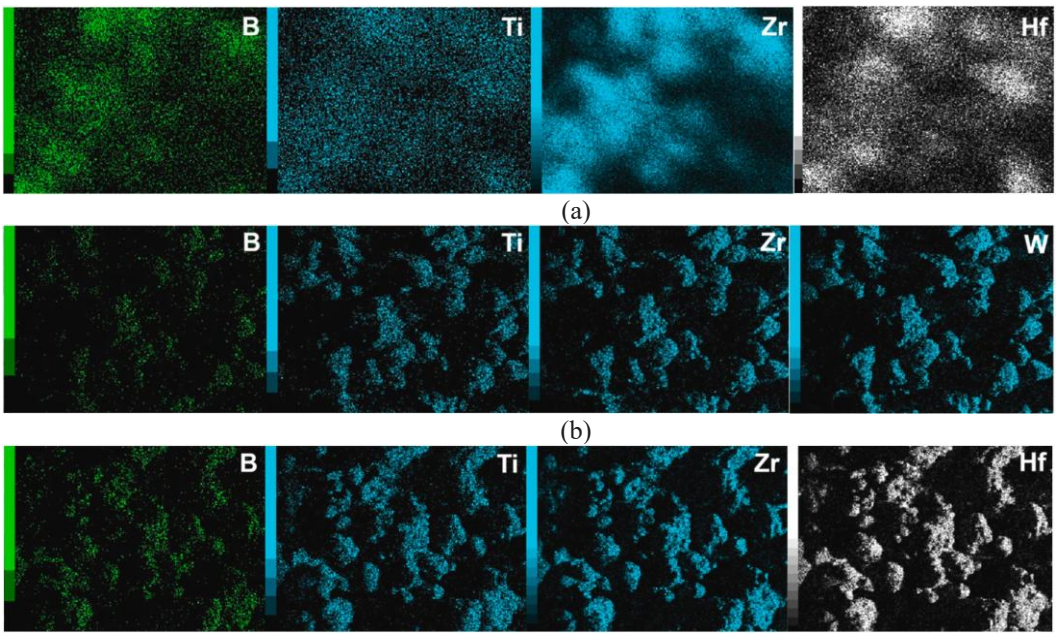

Fig. 3. SEM images and elemental distribution in powders: (a) initial as-blended mixture, (b) after 6 h of milling, and (c) after 10 h of milling [26].

of $(HfTiWZr)B_2$ from constituent borides and elemental boron powder using high-energy ball milling and spark plasma sintering, the boron distribution is clearly observed in the SEM image of the as-blended powders before milling (Fig. 3(a)). At the same time, after only 6 h of milling, the intensity of boron detection sharply decreases (Fig. 3(b)) and becomes very weak after 10 h of powder mixture processing (Fig. 3(c)), whereas the boron distribution is not detected in SEM images and EDS spectral mapping obtained from polished cross-sectional samples.

At the same time, in the HEB $(Ti_{0.2}Zr_{0.2}Hf_{0.2}Nb_{0.2}Ta_{0.2})B_2$ synthesized by boro/carbothermal reduction [15] from a mixture of oxides with B_4C, continuous distributions of boron and oxygen were detected after SPS synthesis of the compacted HEB-0SiC sample (Fig. 5) [15]. This is apparently associated with B_2O_3, which decomposes at temperatures above 3000–3500 °C. This is confirmed by the oxygen content analysis, which showed the presence of 0.81 wt.% and

0.04 wt.% oxygen in the as-synthesized HEB powder and in the sintered HEB-0SiC compact, respectively.

However, EDS mapping of the cross-section of the interface between the reduced HEB-0SiC sample (Fig. 6) [15] and the oxide layer shows that the intensity of the boron distribution in the sample is significantly lower and is associated with similarity to the distributions of niobium and tantalum. At the same time, in the region of intense Zr distribution in the upper part of the examined area, where the contribution of zirconium to the boron distribution is the greatest, a dark contrast is observed. This means that the B Kα emission of the boron spectrum is absent, although boron itself is present in this region. This is due to the fact that the photon energy of the B Kα emission band, hν = 180–190 eV [27, 28], lies in the same energy range as the $M_{4,5}$ absorption edge of X-ray photons ([29], pp. 27, 29; Fig. 6d shows the absorption spectrum in a ZrCo alloy). Therefore, as a result of resonant complete absorption of the B Kα emission band in crystallites containing Zr, a dark background appears when identifying the boron content in them.

Since the decomposition temperature of B_2O_3 is very high, its residues on the surface of HEB crystallites can be avoided during their synthesis by zone melting of simple diborides at temperatures above 3500 °C. Taking these circumstances into account, as well as the substantiated relevance of creating HEB + B_4C composites discussed above, the authors of Ref. [30] obtained a ceramic eutectic composite based on B_4C, directionally reinforced with the high-entropy boride $(TiZrHfNbTa)B_2$. Figure 7 [30] presents EDX mapping of the constituent elements for the directionally solidified eutectic composite (DSCE) $B_4C/(Ti_{0.2}Zr_{0.2}Hf_{0.2}Nb_{0.2}Ta_{0.2})B_2$, demonstrating a distinct distribution of all elements within similarly ordered crystallites against the background of a dark B_4C matrix.

However, in the boron atom distribution, a dark background was observed at the locations of the crystallites against the blue boron distribution corresponding to the B_4C eutectic constituent of the synthesized HEB+B_4C composite. This is associated with the large difference in the intensity of B Kα spectral emission from the crystallites compared with the emission of B Kα photons from B_4C. In the crystallites, these photons are scattered and absorbed by metals, especially zirconium, since the energy of its $M_{4,5}$ absorption edge corresponds to the energy of B Kα radiation, resulting in resonant absorption of these photons.

In boron carbide, B Kα photons are practically not absorbed, since the environment of boron atoms contains four times fewer carbon atoms; moreover, carbon atoms readily transmit B Kα photons because they do not have

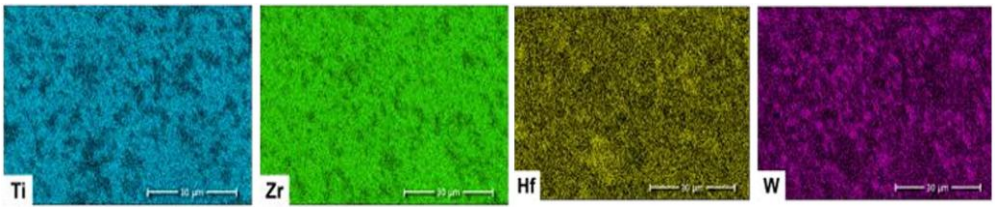

Fig. 4. SEM image and EDS mapping results of cross-sections of sintered boride compacts: 6B-1800 [26].

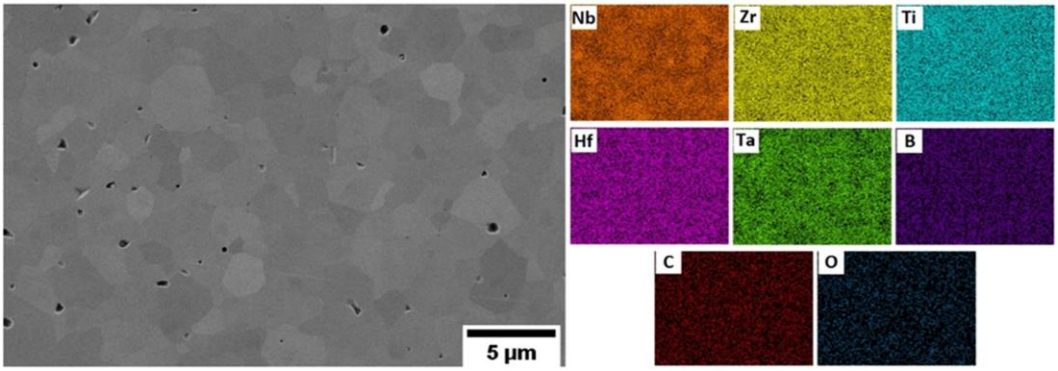

Fig. 5. SEM image and EDS mapping of the sintered HEB-0SiC sample [15].

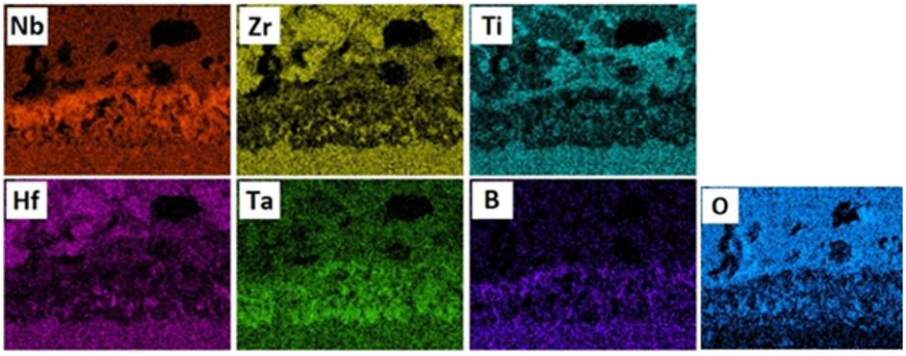

Fig. 6. EDS mapping of the cross-section of the interface between the unoxidized HEB-0SiC sample and the oxide layer after dynamic oxidation at ~2100 °C for 60 s [15].

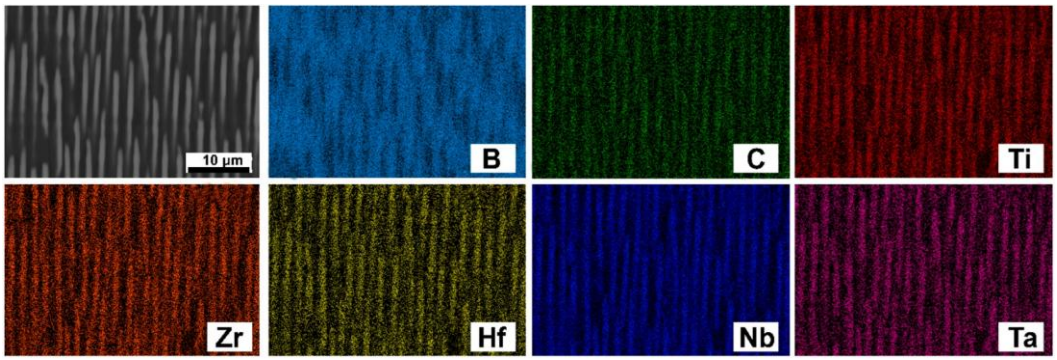

Fig. 7. EDX mapping of the components of the directionally solidified eutectic composite (DSCE) $B_4C/(Ti_{0.2}Zr_{0.2}Hf_{0.2}Nb_{0.2}Ta_{0.2})B_2$ [30].

absorption edges in this energy range.

At the same time, in HEB+SiC composites (Fig. 12 in Ref. [15]), such contrast is absent because there is no other boron-containing substance. Therefore, the boron distribution intensity, although somewhat attenuated by zirconium, is concentrated in the crystallites, where the metal content is increased.

Conclusion

Thus, when analyzing maps of atomic distribution in composite materials, it is necessary to take into account the presence, in the crystallites of the constituent phases of the composites, of atoms with X-ray photon absorption edge energies capable of significantly changing the intensity of the radiation used in X-ray spectral analyzers to determine the distribution and content of material components.

Funding:
This research received no external funding.

Conflict of Interest:
The authors declare no conflicts of interest.

Zaulychnyy Y.V. – Doctor of Physical and Mathematical Sciences, Professor at the Department of High-Temperature Materials and Powder Metallurgy.
Mosiak V.T. – PhD student at the Department of High-Temperature Materials and Powder Metallurgy.
Biriukovych L.O. – Candidate of Technical Sciences, Associate Professor at the Department of High-Temperature Materials and Powder Metallurgy.
Stepanov O.V. – Candidate of Technical Sciences, Associate Professor at the Department of High-Temperature Materials and Powder Metallurgy.
Bogomol Y.I. – Doctor of Technical Sciences, Head of the Department of High-Temperature Materials and Powder Metallurgy.

[1] J.W. Yeh, S.K. Chen, S.J. Lin, J.Y. Gan, T.S. Chin, T.T. Shun, C.H. Tsau, S.Y. Chang, *Nanostructured High-Entropy Alloys with Multiple Principal Elements: Novel Alloy Design Concepts and Outcomes*, Adv. Eng. Mater. 6(5), 299 (2004); https://doi.org/10.1002/adem.200300567.
[2] B. Cantor, I.T.H. Chang, P. Knight, A.J.B. Vincent, *Microstructural development in equiatomic multicomponent alloys,*Mater. Sci. Eng. A 375–377, 213 (2004); https://doi.org/10.1016/j.msea.2003.10.257.
[3] C.M. Rost, E. Sachet, T. Borman, A. Moballegh, E.C. Dickey, D. Hou, J.L. Jones, S. Curtarolo, J.P. Maria, *Entropy-stabilized oxides,* Nat. Commun. 6, 8485 (2015); https://doi.org/10.1038/ncomms9485.
[4] J. Gild, Y. Zhang, T. Harrington, S. Jiang, T. Hu, M.C. Quinn, W.M. Mellor, N. Zhou, K. Vecchio, J. Luo, *High-Entropy Metal Diborides: A New Class of High-Entropy Materials and a New Type of Ultrahigh Temperature Ceramics,* Sci. Rep. 6, 37946 (2016); https://doi.org/10.1038/srep37946.
[5] Y. Zhang, W.M. Guo, Z.B. Jiang, Q.Q. Zhu, S.K. Sun, Y. You, K. Plucknett, H.T. Lin, *Dense high-entropy boride ceramics with ultra-high hardness,* Scr. Mater. 164, 135 (2019); https://doi.org/10.1016/j.scriptamat.2019.01.021.
[6] Y. Zhang, Z.B. Jiang, S.K. Sun, W.M. Guo, Q.S. Chen, J.X. Qiu, K. Plucknett, H.T. Lin, *Microstructure and mechanical properties of high-entropy borides derived from boro/carbothermal reduction,* J. Eur. Ceram. Soc. 39(13), 3920 (2019); https://doi.org/10.1016/j.jeurceramsoc.2019.05.017.
[7] Y. Zhang, S.K. Sun, W. Zhang, Y. You, W.M. Guo, Z.W. Chen, J.H. Yuan, H.T. *Lin, Improved densification and hardness of high-entropy diboride ceramics from fine powders synthesized via borothermal reduction process,* Ceram. Int. 46(9), 14299 (2020); https://doi.org/10.1016/j.ceramint.2020.02.214.
[8] G. Tallarita, R. Licheri, S. Garroni, R. Orrù, G. Cao, Scr. *Novel processing route for the fabrication of bulk high-entropy metal diborides,* Mater. 158, 100 (2019); https://doi.org/10.1016/j.scriptamat.2018.08.039.
[9] G. Tallarita, R. Licheri, S. Garroni, S. Barbarossa, R. Orrù, G. Cao, *High-entropy transition metal diborides by reactive and non-reactive spark plasma sintering: A comparative investigation,* J. Eur. Ceram. Soc. 40(4), 942 (2020); https://doi.org/10.1016/j.jeurceramsoc.2019.10.031.
[10] R. Guo, Z. Li, L. Li, Y. Liu, R. Zheng, C. Ma, *Microstructures and oxidation mechanisms of $(Zr_{0.2}Hf_{0.2}Ta_{0.2}Nb_{0.2}Ti_{0.2})B_2$ high-entropy ceramic,* J. Eur. Ceram. Soc. 42(5), 2127 (2022); https://doi.org/10.1016/j.jeurceramsoc.2021.12.036.

[11] W. Yang, G. Xiao, Z. Ren, *Spark plasma sintering synthesis of ReB2-type medium-entropy diboride $(W_{1/3}Re_{1/3}Ru_{1/3})B_2$ with high hardness,* Scr. Mater. 227, 115299 (2023); https://doi.org/10.1016/j.scriptamat.2023.115299.

[12] J.X. Liu, X.Q. Shen, Y. Wu, F. Li, G.J. Zhang, *Mechanical properties of hot-pressed high-entropy diboride-based ceramics,* J. Adv. Ceram. 9(4), 503 (2020); https://doi.org/10.1007/s40145-020-0383-8.

[13] W. Li, Y. Liu, J. Li, Y. Cao, *Ablation behavior of $(Ti_{0.2}Zr_{0.2}Hf_{0.2}Nb_{0.2}Ta_{0.2})B_2$-SiC-Si ceramics via reactive melt infiltration,* Mater. Charact. 218, 114468 (2024); https://doi.org/10.1016/j.matchar.2024.114468.

[14] H. Ying, Q.L. Guo, B.W. Yuan, H.Z. Fan, W. Yan, X. Zheng, J. Zhang, J.W. Wu, R.H. Liu, *Preparation and properties of Ta foil toughened high entropy $(Ti_{0.2}Zr_{0.2}Hf_{0.2}Nb_{0.2}Ta_{0.2})B_2$-SiC layered structure composites,* Mater. Today Commun. 42, 111466 (2025); https://doi.org/10.1016/j.mtcomm.2024.111466.

[15] V. Kombamuthu, H. Ünsal, Z. Chlup, M. Tatarkova, A. Kovalcíkova, I. Zhukova, N. Hosseini, M. Hičák, I. Dlouhý, P. Tatarko, *Effect of SiC on densification, microstructure and mechanical properties of high entropy diboride $(Ti_{0.2}Zr_{0.2}Hf_{0.2}Nb_{0.2}Ta_{0.2})B_2$,* J. Eur. Ceram. Soc. 44(9), 5358 (2024); https://doi.org/10.1016/j.jeurceramsoc.2023.12.072.

[16] Q.L. Guo, H. Ying, B.W. Yuan, H.Z. Fan, L. Hua, R.H. Liu, *Preparation and properties of Ta fiber reinforced high-entropy $(Ti_{0.2}Zr_{0.2}Hf_{0.2}Nb_{0.2}Ta_{0.2})B_2$-SiC composite ceramics,* J. Wang, Ceram. Int. 50(24), 56070 (2024); https://doi.org/10.1016/j.ceramint.2024.09.266.

[17] Y. Yang, J.Q. Bi, K.N. Sun, Y.G. Chen, *Toughened bulk high-entropy diborides with high hardness and enhanced oxidation resistance via SiC whiskers,* Mater. Charact. 210, 113814 (2024); https://doi.org/10.1016/j.matchar.2024.113814.

[18] W. Hao, X.Z. Lu, L. Li, J.X. Liu, F. Li, G.J. Zhang, *Toughened (Ti0.2Zr0.2Hf0.2Nb0.2Ta0.2)B2–SiC composites fabricated by one-step reactive sintering with a unique SiB6 additive,* J. Adv. Ceram. 13(1), 86 (2024); https://doi.org/10.26599/JAC.2024.9220838.

[19] X.Q. Shen, J.X. Liu, F. Li, G.J. Zhang, *Preparation and characterization of diboride-based high entropy $(Ti_{0.2}Zr_{0.2}Hf_{0.2}Nb_{0.2}Ta_{0.2})B_2$–SiC particulate composites,* Ceram. Int. 45(18), 24508 (2019); https://doi.org/10.1016/j.ceramint.2019.08.178.

[20] Y.J. Shi, W.X. Li, X.R. Zhang, Z.X. Zhang, *Preparation and toughening mechanism of Al_2O_3 composite ceramics toughened by B_4C@TiB_2 core–shell units,* J. Adv. Ceram. 12(12), 2371 (2023); https://doi.org/10.26599/JAC.2023.9220826.

[21] L.Y. Xiang, L.F. Cheng, L. Shi, X.Y. Yin, L.T. Zhang, J. Alloys Compd. 638, 261 (2015).

[22] Z.L. Huo, X. Wu, C.F. Du, J. Yang, Ceram. Int. 50(21), 43927 (2024).

[23] H. Ying, Q. Guo, Y. Wen, B. Yuan, J. Wu, J. Wang, *Toughening and high-temperature self-lubricating of high-entropy boride ceramics through h-BN,* J. Adv. Ceram. 14(8), 9221120 (2025); https://doi.org/10.26599/JAC.2025.9221120.

[24] D. Wang, K. Xu, Q. Li, X. Ding, S. Ran, *Microstructure and Mechanical Properties of In-Situ B4C-(TiZrHfNbTa) B2 Composite by Reactive Spark Plasma Sintering*, JOM 74, 4129 (2022); https://doi.org/10.1007/s11837-022-05377-y.

[25] J. Gu, J. Zou, S.K. Sun, H. Wang, S.Y. Yu, J. Zhang, W. Wang, Z. Fu, *Dense and pure high-entropy metal diboride ceramics sintered from self-synthesized powders via boro/carbothermal reduction approach,* Sci. China Mater. 62(12), 1898 (2019); https://doi.org/10.1007/s40843-019-9469-4.

[26] S. Kavak, K.G. Bayrak, M. Mansoor, M. Kaba, E. Ayas, Ö. Balcı-Çağıran, B. Derin, M.L. Öveçoğlu, D. Ağaoğulları, *First principles calculations and synthesis of multi-phase $(HfTiWZr)B_2$ high entropy diboride ceramics: Microstructural, mechanical and thermal characterization,* J. Eur. Ceram. Soc. 43(3), 768 (2023); https://doi.org/10.1016/j.jeurceramsoc.2022.10.047.

[27] J.A. Bearden, *X-Ray Wavelengths,* Rev. Mod. Phys. 39(1), 78 (1967); https://doi.org/10.1103/RevModPhys.39.78.

[28] M.A. Blokhin, I.G. Shveitser, X-ray Spectral Handbook (Nauka, Moscow, 1982).

[29] Y. Piao, Q. Jiang, H. Li, J. Liang, H. Matsumoto, Y. Sato, J. Zhang, Y. Chen, *Identify Zr Promotion Effects in Atomic Scale for Co-Based Catalysts in Fischer–Tropsch Synthesis,* ACS Catal. 10(14), 7894 (2020); https://doi.org/10.1021/acscatal.0c01874.

[30] I. Bogomol, E. Ferkhatly, S. Ponomarchuk, Y. Zaulychnyi, M. Karpets, I. Solodkyi, *Ceramic eutectic composites based on B_4C directionally reinforced by high-entropy $(TiZrHfNbTa)B_2$ boride*, J. Eur. Ceram. Soc. 44(1), 51 (2024); https://doi.org/10.1016/j.jeurceramsoc.2023.08.028.

Я.В. Зауличний, В.Т. Мосяк, Л.О. Бірюкович, О.В. Степанов, Ю.І. Богомол

Особливості виявлення бору та інтерпретації його розподілу у високоентропійних боридах і композитах на основі B_4C: короткий огляд

Національний технічний університет України "Київський політехнічний інститут імені Ігоря Сікорського", м. Київ, Україна, m.vasyl-imz24@lll.kpi.ua

Інтерпретація розподілу бору у високоентропійних диборидних кераміках і композитах на основі B_4C залишається складним завданням через низьку енергію B Kα-випромінювання та його взаємодію з важкими металевими елементами. У цій роботі проаналізовано літературні дані щодо EDS- та WDS-картування елементів у високоентропійних боридах і композитах B_4C–(TiZrHfNbTa)B_2 з метою визначення чинників, які впливають на виявлення бору. Особливу увагу приділено впливу перехідних металів на інтенсивність сигналу бору. Показано, що видиме збіднення бором у кристалітах високоентропійних диборидів, яке спостерігається на елементних картах, не обов'язково свідчить про його реальну відсутність. Зменшення інтенсивності B Kα-сигналу пов'язане з процесами поглинання та розсіювання, що відбуваються в боридних кристалітах. Значний внесок у цей ефект можуть робити цирконійвмісні фази, для яких $M_{4,5}$-край поглинання розташований близько до енергетичного діапазону характеристичного випромінювання бору. Отримані результати демонструють, що для достовірної інтерпретації розподілу бору в багатофазних боридних системах необхідно враховувати ефекти поглинання рентгенівського випромінювання. Ці чинники слід брати до уваги під час аналізу елементних карт високоентропійних боридів і B_4C-вмісних композитів.

Ключові слова: високоентропійні бориди, карбід бору, EDS-картування, WDS-картування, розподіл бору, B Kα-випромінювання, поглинання рентгенівського випромінювання, високоентропійна кераміка, композити B_4C–(TiZrHfNbTa)B_2.